ORIGINAL PAPER

Exploring free energy profile of petroleum thermal cracking mechanisms

Feng Wang[1] · Peng Tao[1]

Abstract
Understanding the mechanisms of petroleum thermal cracking is critical to develop more efficient and eco-friendly petroleum cracking processes. Asphaltenes are the main component of petroleum subjected to cracking processes. Thermal cracking mechanisms of petroleum were explored by computational methods using 1,2-diphenylethane (DPE) as a model molecule in this study. The overall mechanisms were divided into four steps including initiation, H-transfer reaction, H-ipso reaction, and termination represented by seven reactions. We carried out extensive quantum chemistry calculations at high levels of theory to accurately explore the minimum energy pathways as the mechanisms of the proposed reactions. The reaction energy and barriers in terms of enthalpy and free energy and their temperature dependence were calculated in the vacuum and in both polar and nonpolar solvents using the polarizable continuum model (PCM) method. The temperature dependence of the target reaction barriers are characterized in different environments and provides computational guidance for future development for petroleum thermal cracking. As the first reported systematic investigation of petroleum cracking mechanisms, this study provided a comprehensive theoretical description of petroleum cracking processes with valuable information about temperature and solvent dependence.

Keywords Thermal cracking mechanisms · Petroleum · Asphaltene · Reaction pathway · Free energy profile

Introduction

Petroleum is a naturally occurring mixture containing thousands of different compounds with wide range of molecular weight [1–3]. Through thermal cracking process, the heavy weight constituents can be converted into lower weight products. The part of light weight products will be further refined before its launch on the market [4, 5]. Petroleum is a complicated mixture with a wide range of fractional compositions. In general, petroleum is consisted of four main components including asphaltenes, resins, saturates, and aromatics [6].

The thermal decomposition of organic molecules have been studied for many decades [7]. For example, theories of bond energies and bond strength related to each constituent were studied to determine the reactivity and thermal stability

of petroleum [4, 8]. Also, the stereochemistry is an important factor on the reactivity and properties for organic molecule [9]. Because the thermal decomposition of petroleum is a complicated process, mechanistic understanding of this process is essential for improving the refinery operations. Therefore, more economic and environment friendly thermal cracking process could be developed and drive the development of modern petrochemical industry [10].

To achieve this goal, it is necessary to delineate petroleum thermal cracking mechanisms for improving cracking process with higher efficiency. In general, thermal cracking of petroleum includes catalytic cracking and hydrocracking. A catalytic cracking is an ionic process aided by a catalyst [11–13], and hydrocracking needs a hydrogen-rich environment [4, 14]. Both catalytic and hydrocracking experimental and theoretical studies have been active during the past several decades [7, 15, 16].

In early studies, many industrial variables including temperature, pressure, and time were controlled to adjust a cracking process and produce different types of products and residues for further processing [17–19]. In many experimental studies, the variable controlling method is still a primary

✉ Peng Tao
  ptao@smu.edu

[1] Department of Chemistry, Center for Scientific Computation, Center for Drug Discovery, Design, and Delivery (CD4), Southern Methodist University, Dallas, TX 75275, USA

choice. For example, the large components in petroleum with molecular weights between 534 and 763 g/mol in liquid were investigated under the temperature from 365 to 420 °C to reveal the selectivity and the nature of addition products [20]. It was found that when the light components of petroleum such as n-alkanes were generated, some of the complex heavy components in the asphaltenes were also produced. In another research, a kinetic model with 132 free-radical reactions were proposed to describe the thermal cracking of tetralin [21]. The model was tested with the experimental data in the temperature range of 350–500 °C. It was revealed that the formation of 1-methylindole decreased with the temperature, whereas the other two formations of n-butylbenzene and naphthalene increased during the process of tetralin thermal cracking. Building a kinetic model with a number of reactions in a specific pressure and over a temperature range were also used in a study describing n-butylcyclohexane thermal cracking process at high pressure 100 bar and in the temperature range of 375–425 °C [22]. It was shown that in the thermal cracking of n-butylcyclohexane, both alkanes and cycloalkanes were generated by the breaking of the side alkyl chain. Controlling temperatures and pressures are often used to test the proposed kinetic model based on the experimental data.

Catalytic cracking can be very efficient to improve the cracking performances and has been studied extensively, with many catalysts proposed. For example, Ni-Pd nanocatalysts were studied in the catalytic thermal cracking of n-C_7 asphaltenes [23]. It is proven that the Ni-Pd nanocatalysts improved the performance of a cracking process. Another example is zeolites. The effects of zeolites frameworks and structure on the performance of alkane cracking process has been studied during the past 70 years. In addition, computational methods were also employed to delineate the catalytic mechanisms and predict the effect of catalyst composition on petroleum cracking [24].

For theoretical investigation of petroleum thermal cracking mechanisms, quantum chemistry methods serve as the main approaches [25–28]. Petroleum as a complicated mixture and its thermal cracking processes with large number of elementary reactions represent major computational challenges. To overcome these, many theoretical works were carried out through modeling molecules to represent main components in a mixture [29–31]. For example, as an asphaltene model molecule, Quinolin-65, has been investigated including the thermal decompositions and interactions between the model molecules. As the result, a new reaction pathway in Quinlin-65 and 1,3-hydrogen shift mechanism was proposed [32]. In another study, coal structures were represented as different functional groups, including oxygen-containing groups, aliphatic hydrocarbon groups, sulfur-containing groups, nitrogen-containing groups, and free radicals [33, 34]. It was

reported that the aliphatic hydrocarbon groups should be further explored in the reaction mechanism of spontaneous combustion of coal.

Most thermal cracking reactions are free radical reactions and could be divided into initiation, propagation, and termination stages [35, 36]. Propane and butane have been used as molecular models for the theoretical studies of the petroleum pyrolysis in hydrogen thermal plasma using density functional theory (DFT) [37]. In another study, hydrogen atoms reacting with toluene and ethyl radical reacting with 4-ethyltoluene were studied to explicate a plasma-driven catalytic hydrogenation mechanism using DFT methods [38]. Also, the bond-dissociation energy of C-C scission and reaction barrier energy of the hydrocarbon thermal cracking were calculated by DFT and Møller-Plesset perturbation theory (MP2) methods [39] In these theoretical studies, the reaction mechanisms with detailed structural, energetic information, reaction pathway were obtained. [28, 40–43]

Although with much in depth information about the reaction mechanisms, the molecules being used for thermal cracking processes thus far are oversimplified models without appropriate representation of the actual chemical processes. 1,2-diphenylethane (DPE) (Scheme 1) is a model molecule used in an investigation of the asphaltenes (one significant fraction of petroleum [44–46]) thermal cracking reaction [47]. This relatively simple model molecule with two benzene rings as terminal groups well represents the chemical complexity of asphaltenes in general. Therefore, using DPE as a model system could provide a new insight into the asphaltenes thermal cracking processes. In this study, using DPE as the model molecule, the asphaltenes cracking reactions mechanisms are computationally investigated in details using various levels of theory including DFT, Møller-Plesset perturbation theory, coupled cluster, and complete basis set composite methods. The elementary reaction steps including initiation, H-transfer, H-ipso, and termination are characterized through intrinsic reaction coordinates method with both energetic and structural information. The solvent and temperature dependence of enthalpy and free energy barriers of these reactions are also investigated. The systematic investigation on petroleum cracking mechanisms could provide a theoretical foundation for radical reactions and future experimental studies. The remaining of the article is organized as materials and methods section, "Results and discussion" section, followed by a brief conclusion section.

Theoretical background

DPE, representing a main structural feature of asphaltene (Scheme 1), is used as the model molecule to study the thermal cracking reaction of asphaltene. The DPE thermal cracking mechanism including initiation, H-transfer reaction, H-

Scheme 1 The chemical formulas of asphaltene and 1,2-diphenylethane (DPE)


Asphaltene   1,2-diphenylethane
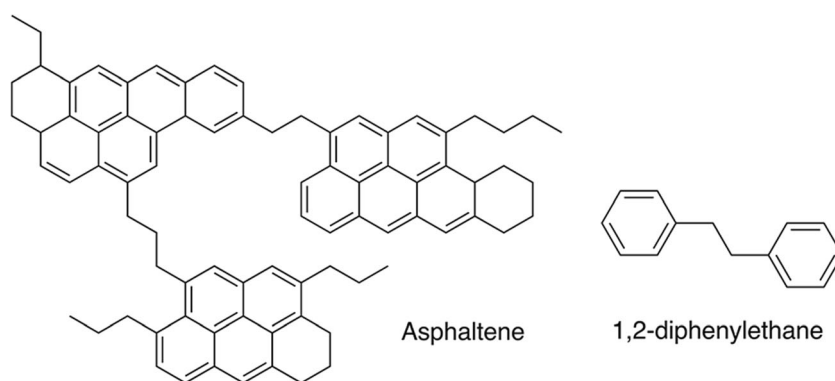
ipso reaction, and termination stages are represented by seven elementary reactions illustrated in Scheme 2 [47]. Reactions (4) and (5) have been referenced as "hydrocracking" reactions. The mechanistic sequences of reactions (4) and (5) were first proposed in thermolysis of toluene as a path for dealkylation

[48]. Since the initial H atom in reaction (4) attacked an ipso position on DPE, in this study, reactions (4) and (5) are referred to as H-ipso reaction in Scheme 2. All seven reactions are subjected to detailed computational studies at various levels of theory.

Scheme 2 The mechanism of thermal cracking including initiation, H-transfer, H-ipso, and termination from reactions (1)–(7)
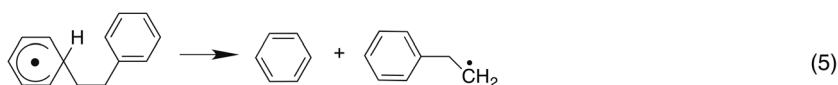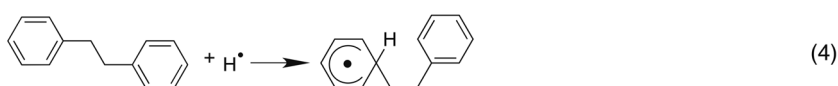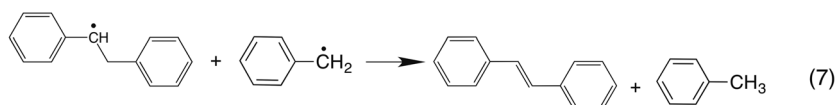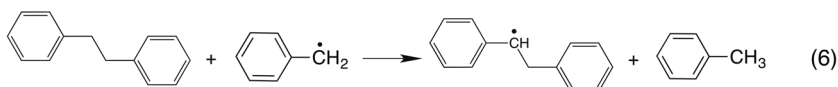
1. Initiation

$$(1)$$

2. H-tranfer reaction

$$(2)$$

$$(3)$$

3. H-ipso reaction

$$(4)$$

$$(5)$$

4. Termination

$$(6)$$

$$(7)$$
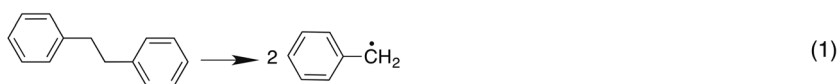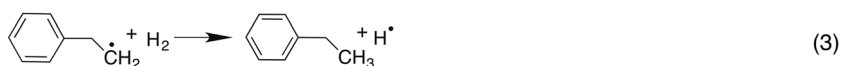
The geometry optimizations were carried out using unrestricted Becke's three-parameter Lee-Yang-Parr (uB3LYP) functional as a hybrid DFT method [49–52], MP2 [53–57], coupled cluster single and double with perturbative triple (CCSD(T)) method [58–61], and a complete basis set method (CBS-QB3) [62, 63]. Intrinsic reaction coordinate (IRC) method [64, 65] are employed to characterize minimum energy pathways (MEPs) for elementary reactions at uB3LYP and MP2 levels of theory with 6–31+G(d,p) basis set. The optimized geometries were subjected to single points energy calculations at uB3LYP/aug-cc-pvtz and CCSD(T)/6–311+G(d,p) levels of theory. In addition, the polarizable continuum model (PCM) is used to calculate the free energy and enthalpy barriers with water and toluene as solvents, respectively, in temperature range from 0 to 800 K at uB3LYP/6–31+G(d,p) level of theory. All calculations were carried out using Gaussian16. [66].

Results and discussion

Initiation reaction of DPE thermal cracking

Reaction (1) of hemolytic C-C bond dissociation leading to two radicals represents a transformation between a closed shell singlet state and an open shell triplet state. To explore the potential energy surface of both states, the energy profiles of the C-C bond breaking were calculated at uB3LYP/6–31+G(d,p) level of theory and plotted in Fig. 1a. The energy profiles of the singlet and triplet states cross at point with C-C distance as 2.96 Å with energy around 62 kcal/mol with regard to singlet ground state. The energy profile in triplet state has an energy peak, and the energy of singlet state increases

monotonously along the elongated C-C bond length. The atoms are labeled in Fig. 1b.

Potential energy profile of DPE thermal cracking

The energy profiles of reactions (1)–(6) at various levels of theory are plotted in Fig. 2a–f, including the energies of reactant, transition state, and product geometries. The reaction barriers and reaction energies of reactions (1)–(6) are listed in the Table 1 as $\Delta E^{\ddagger}$ and ΔE, respectively. The energy profiles are calculated using four levels of theory including B3LYP, MP2, CBS-QB3, and CCSD methods with 6–31G+(d,p) basis set.

For reaction (1) of homolytic C-C bond dissociation leading to two radicals, a high reaction barrier is calculated at B3LYP/6–31G+(d,p) level of theory due to the transformation from a singlet reactant to a triplet product (Fig. 2a). The energy of reactant geometry is obtained in the singlet state. The geometry of transition state is approximated as a triplet state in the intersection of singlet and triplet energy profiles. This reaction is very endothermic with reaction energy around 60 kcal/mol to essentially break C-C single bond.

For reaction (2), in which benzyl radical extracts a hydrogen atom from H_2 molecule to produce a toluene and regenerate a H• radical, the barriers calculated by MP2, B3LYP, and CBS-QB3 methods are close to each other within 1 kcal/mol range (Table 1 and Fig. 2b). CCSD method overestimates the barrier by about 14 kcal/mol comparing to the other three methods. This reaction is rather endothermic based on the results from CCSD, B3LYP, and CBS-QB3 methods. However, the MP2 results suggest that this step reaction is only slightly endothermic by more than 2.2 kcal/mol.

The reaction (3), in which 2-phenylethyl free radical extracts a hydrogen atom from H_2 molecule to produce
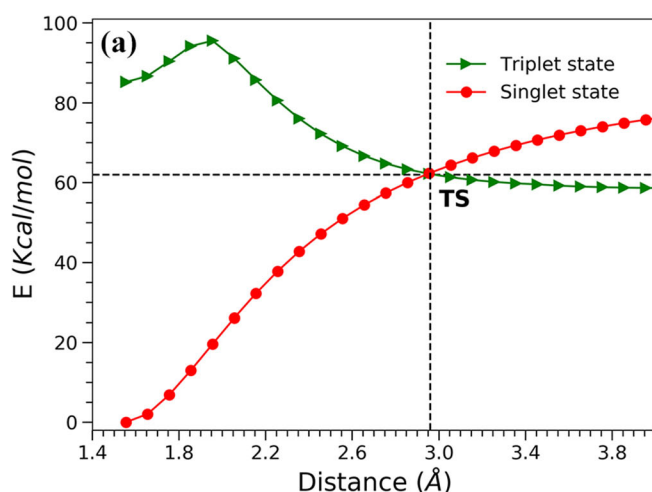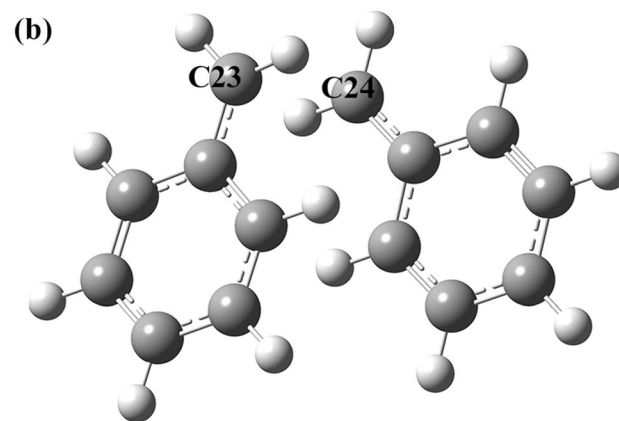

Fig. 1 Computational results of reaction (1). **a** The energy profile along scanning the distance between C23 and C24 of DPE at B3LYP/6–31+G(d,p) level of theory, in the triplet state (green triangle) and the singlet state (red round dot). **b** The geometries of two radicals at the intersection point on the singlet surface

ethylbenzene and regenerate a H• radical, is chemically similar to the reaction (2). The reaction barrier calculated by four different methods ranges from 10.7 kcal/mol using B3LYP functional to 16.4 kcal/mol using CCSD method (Fig. 2c). This reaction is endothermic based on CCSD, B3LYP, and CBS-QB3 methods. For MP2 method, the results indicate that reaction (3) is exothermic by less than 5 kcal/mol.

The reaction (4), in which H• radical binds with DPE to produce a new radical, is an exothermic reaction with a low reaction barrier, which is shown by the calculations using B3LYP, MP2, and CBS-QB3 methods in Fig. 2d. The calculated barriers range from effectively 3.8 kcal/mol using MP2 method to 18.9 kcal/mol using CBS-QB3 method (Table 1). The exothermicity of this step of reaction is also shown by all

three levels of theory ranging between − 15.4 and − 25.8 kcal/mol.

The barriers generated by B3LYP and CBS-QB3 methods of reaction (5), in which radical product of reaction (4) breaks into benzene and 2-phenylethyl free radical, are 18.6 kcal/mol and 22.1 kcal/mol, respectively, with difference as 3.5 kcal/mol. As comparison, the MP2 method overestimates the barriers by about 10 kcal/mol higher than B3LYP method. The reaction (5) is endothermic based on the results of both B3LYP and CBS-QB3 methods, but exothermic based on the result of MP2 method.

In the reaction (6), benzyl radical extracts a hydrogen atom from DPE to produce toluene and generate another radical. Due to the chemical complexity, only B3LYP calculations
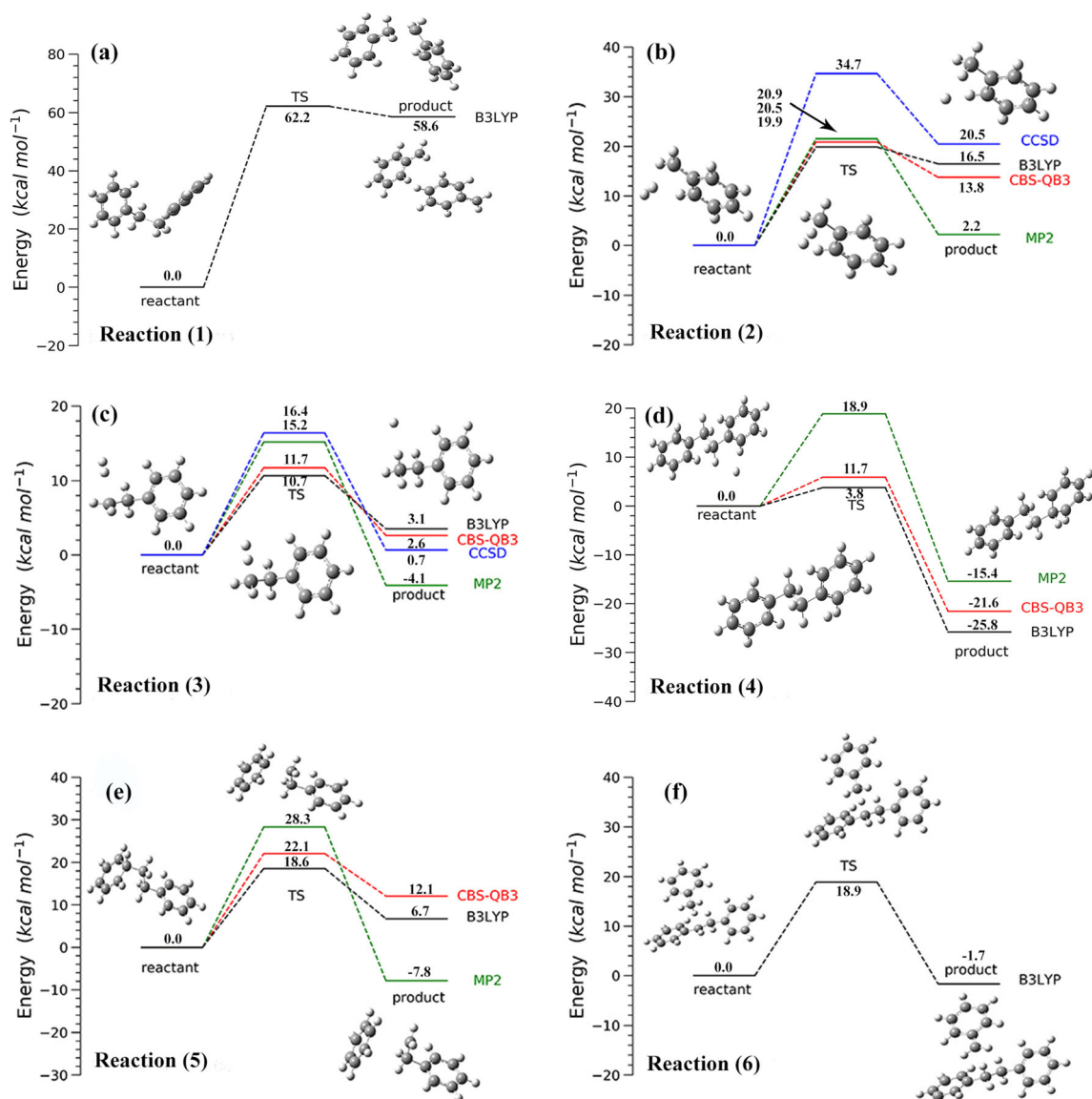

Fig. 2 Energy profiles of reactant, transition state and product geometries of reactions (1)–(6) after being optimized at B3LYP (black line), MP2 (green line), and CCSD (blue line) with 6–31G+(d,p) basis set and CBS- QB3 (red) levels of theory. **a** Reaction (1). **b** Reaction (2). **c** Reaction (3). **d** Reaction (4). **e** Reaction (5). **f** Reaction (6). The reported energies are in kcal/mol

Table 1 Reactions (1)–(7) in B3LYP, MP2, CBS-QB3, and CCSD methods with 6–31G+ (d,p) basis set. $\Delta E^{\ddagger}$ represents the reaction barrier (kcal/mol), ΔE represents the reaction energies (kcal/mol)

Reaction barriers/energies (kcal/mol)	B3LYP		MP2		CBS-QB3		CCSD	
	$\Delta E^{\ddagger}$	ΔE	$\Delta E^{\ddagger}$	ΔE	$\Delta E^{\ddagger}$	ΔE	$\Delta E^{\ddagger}$	ΔE
Reaction (1)	62.2	58.6	---	----	----	----	---	---
Reaction (2)	19.9	16.5	20.5	2.2	20.9	13.8	34.7	20.5
Reaction (3)	10.7	3.5	15.1	− 4.1	11.7	2.6	16.4	0.7
Reaction (4)	3.8	− 25.8	18.9	− 15.4	5.9	− 21.6	---	---
Reaction (5)	18.6	6.7	28.3	− 7.8	22.1	12.1	---	---
Reaction (6)	18.9	− 1.7	---	---	---	---	---	---
Reaction (7)	7.4	− 48.5	---	---	---	---	---	---

were successfully completed for reaction (6). This step of reaction has 18.9 kcal/mol barrier and is slightly exothermic by less than about 1.6 kcal/mol.

The reaction (7) represents a transformation between a closed shell singlet state and an open shell triplet state (Scheme 2). To explore the potential energy surface of both states, the energy profiles of the H-transfer reaction were calculated at uB3LYP/6–31+G(d,p) level of theory and plotted in Fig. 3a. The energy profiles of the singlet and triplet states cross at the C9-H15 distance as 1.81 Å with energy around 55 kcal/mol with regard to singlet ground state. The energy profile of the crossing point is represented as transition state in Fig. 3b. The reaction energy in Fig. 3b shows that the reaction (7) is exothermic with reaction energy as − 48.5 kcal/mol (Table 1).

In this thermal cracking process of DPE, the generation of H atoms is a key issue since the high bond dissociation energy of H_2 (104 kcal/mol) makes it an unlikely source of hydrogen atom radicals [48]. Therefore, an initial reaction with H_2 molecule to form a hydrogen atom is necessary, such as the H-transfer reactions (2) and (3). In 1980, it was discovered that the thermolysis reaction of DPE produced benzyl radicals, and

the consequence reaction in the presence of H_2 produced benzene and ethylbenzene [67]. Accordingly, the reactions (1–5) in Scheme 2 are proposed as reaction mechanism for the DPE thermolysis. The key steps of this proposed mechanism are H-transfer and H-ipso reactions, which are also referred to as hydrocracking process and were identified as a path for dealkylation in the thermolysis of toluene. It was proposed that benzyl radicals generated by reaction (1) are more favorable to react with the DPE (reaction (6)) rather than with H_2 (reaction (2) or (3)), since the bond dissociation energy for the H-H bond (104 kcal/mol) is greater than the C-H bond (86.1 kcal/mol) in DPE [48]. Our calculations of the reactions (2) and (6) listed in Table 1 also support this. The barriers for reactions ((2), (3), and (6)) are rather low, suggesting that these are not kinetically controlled reactions. Based on the energies calculated by various levels of theory, reaction (6) is likely to be an exothermic reaction. Reactions ((2) and (3)) are likely to be endothermic, and are more thermodynamically favorable than reaction (6).

The single point energy profiles of reactant, transition state, and product at high levels of theory, uB3LYP/aug-cc-pvtz and CCSD(T)/6-311G+(d,p), are plotted in the Fig. 4. The
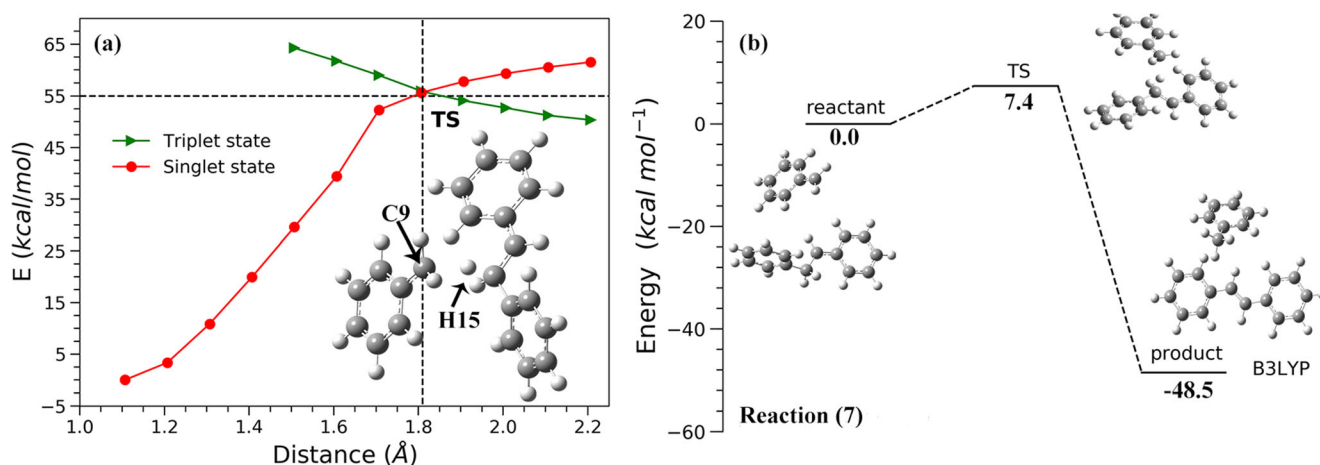

Fig. 3 Computational results of reaction (7). **a** The energy profile along scanning the distance between C9 and H15 of DPE at B3LYP/6–31+ G(d,p) level of theory, in a triplet state (green triangle), and a singlet state (red round dot). The geometry of TS is labeled adjacent to the interaction on the singlet surface. **b** The energy profiles of reactant, transition state and product geometries of reaction (7) after being optimized at B3LYP with 6–31+G(d,p) basis set. The reported energies are in kcal/mol
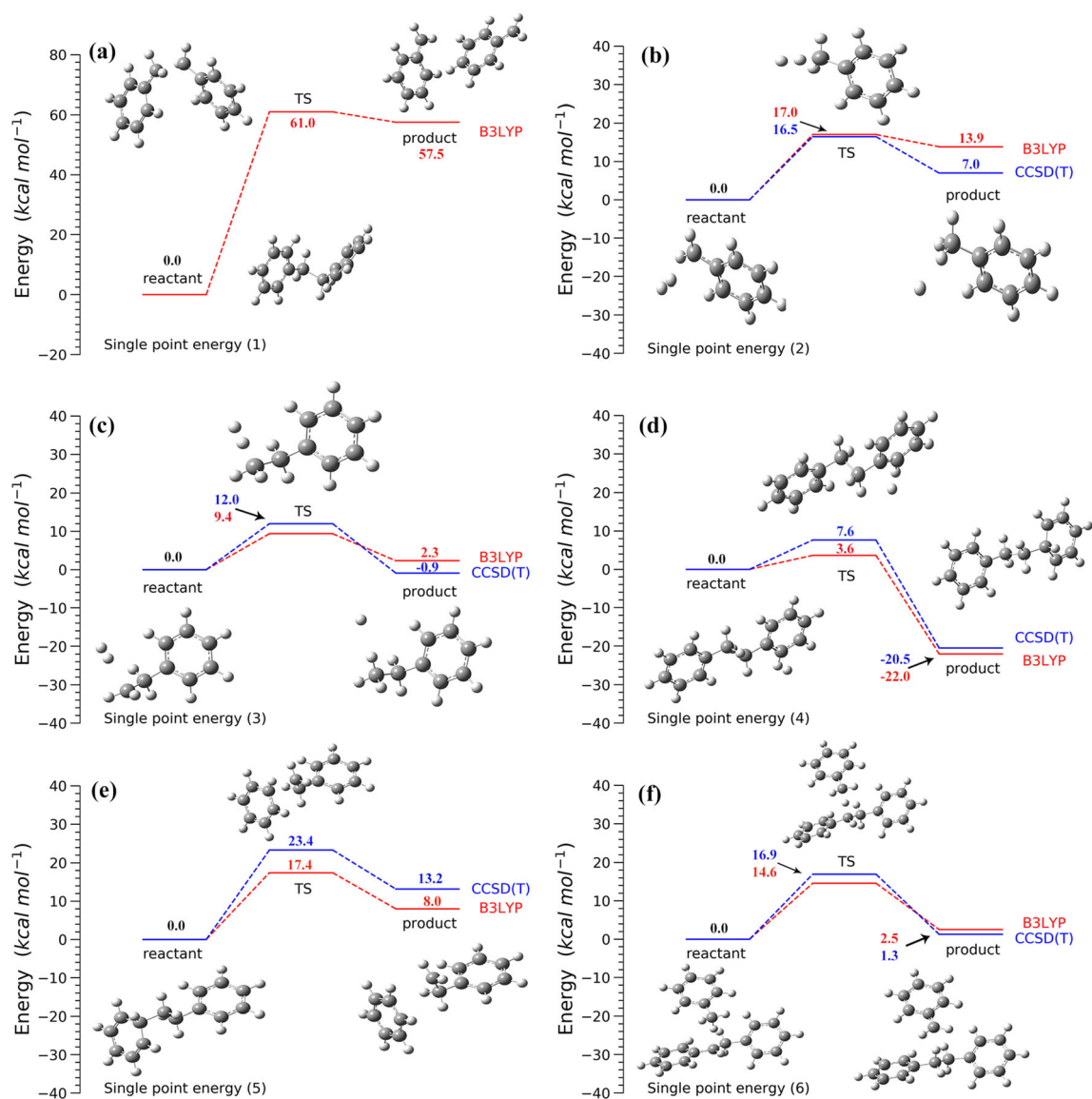
Fig. 4 The single point energies of reactant, transition state and product geometries along the reaction pathway (1)–(6) at uB3LYP/aug-cc-pvtz (red line) and CCSD(T)/6–311+G(d,p) (blue line) levels of theory

geometries optimized by uB3LYP level theory were used to produce the single point energy values. The reaction barriers and energies of reactions ((1)–(6)) are listed in Table 2.

For reaction (1), the high energy barrier obtained using a smaller basis set is confirmed at uB3LYP/aug-cc-pvtz level of theory. This reaction is very endothermic. For reaction (2), the single point energy barriers generated at two levels of theory

Table 2 The single point energies of reactant, transition state, and product for pathways (1–6) at uB3LYP/aug-cc-pvtz and CCSD(T)/6–311+G(d,p) levels of theory. $\Delta E^{\ddagger}$ represents the reaction barrier (kcal/mol), ΔE represents the reaction energies (kcal/mol)

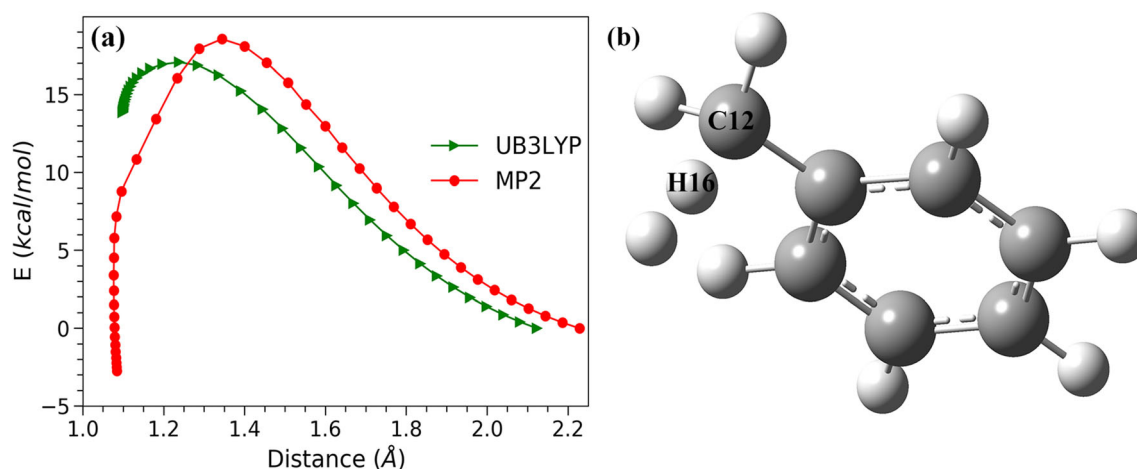| Reaction barriers/energies (kcal/mol)	uB3LYP/aug-cc-pvtz		CCSD(T)/6-311G+(d,p)	
	$\Delta E^{\ddagger}$	ΔE	$\Delta E^{\ddagger}$	ΔE
Reaction (1)	61.0	57.5	---	---
Reaction (2)	17.0	13.9	16.5	7.0
Reaction (3)	9.4	2.3	12.0	− 0.9
Reaction (4)	3.6	− 22.0	7.6	− 20.5
Reaction (5)	17.4	8.0	23.3	13.2
Reaction (6)	14.6	2.5	16.9	1.3

Fig. 5 The minimum energy pathways of reaction (2). **a** Energetic profiles using uB3LYP (green triangle) and MP2 (red round dot) methods with 6–31+G(d,p) basis set. **b** The transition state geometry optimized at uB3LYP/6–31+G(d,p) level of theory with labels of C12-H16. The distance between C12 and H16 is the key atomic distance of x-axis in (**a**)

are close to each other around 17 kcal/mol within 1 kcal/mol range (Table 2). This reaction is endothermic based on both methods. The reaction (3) barriers from single point calculations around 10 kcal/mol agree with the ones calculated at uB3LYP/6–31G+(d,p) and CBS-QB3 methods, and is lower than the ones calculated at MP2 and CCSD with 6–31G+(d,p) basis set. Reaction (3) is slightly exothermic by less than about 0.6 kcal/mol based on uB3LYP/aug-cc-pvtz method, and is a slightly endothermic reaction based on the CCSD(T)/6–311G+(d,p) method. Therefore, it is likely that this reaction is close to thermodynamically neutral.

Reaction (4) is rather exothermic (Fig. 4d) according to both uB3LYP and CCSD(T) methods with reaction barrier lower than 8 kcal/mol, which is in the agreement with the energy profiles illustrated in Fig. 2d. Both levels of theory show that this reaction is endothermic. It is likely that reaction (4) is the main driving reaction of cracking process with the significant exothermicity. For reaction (5), the single point

energy barrier is 17.4 kcal/mol and 23.3 kcal/mol using uB3LYP/aug-cc-pvtz and CCSD(T)/6–311G+(d,p), respectively (Fig. 4e and Table 2). For reaction (6), uB3LYP/aug-cc-pvtz and CCSD(T)/6–311G+(d,p) method results are consistent in both reaction barrier and reaction energies. This reaction has barrier around 15 kcal/mol and is slightly endothermic with reaction energy under 3 kcal/mol (Fig. 4f and Table 2).

The minimum energy pathways of H-transfer, H-ipso, and termination reactions

The MEPs of H-transfer, H-ipso, and termination including reactions (2)–(5) are constructed using IRC method and plotted and illustrated in Figs. 5, 6, 7, and 8. The MEPs of reactions (2)–(4) were generated by both MP2 and DFT methods with 6–31G+(d,p) basis set. The MEP for reaction (5) was obtained at B3LYP/6–31G+(d,p) level of theory only.
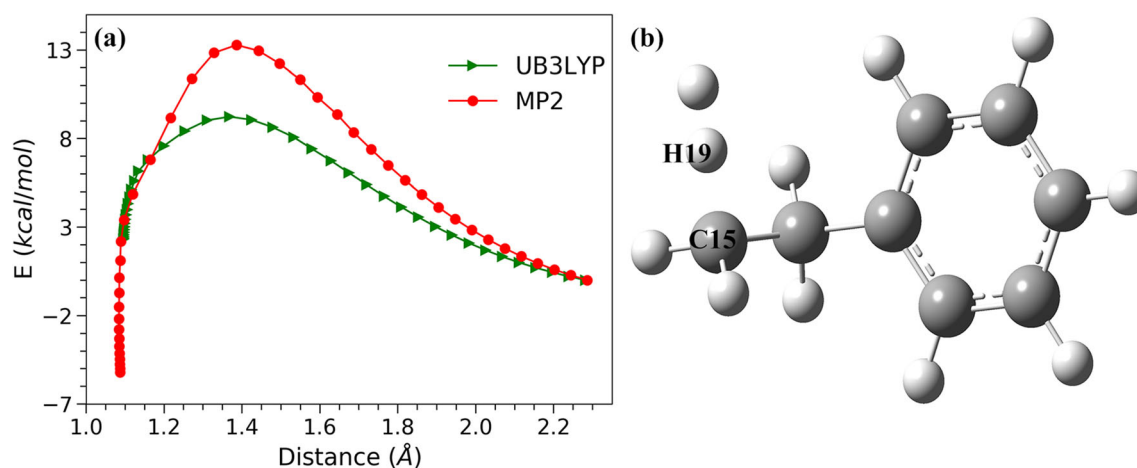

Fig. 6 The minimum energy pathways of reaction (3). **a** Energetic profiles using uB3LYP (green triangle) and MP2 (red round dot) methods with 6–31+G(d,p) basis set. **b** The transition state geometry optimized by uB3LYP/6–31+G(d,p) level of theory with labels of C15-H19. The distance between C15 and H19 is the x-axis in (**a**)
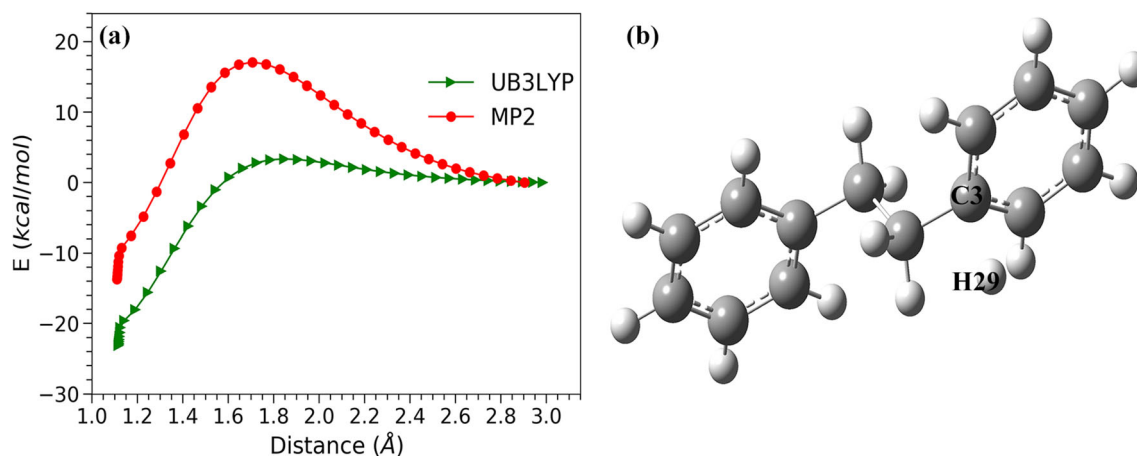
Fig. 7 The minimum energy pathways of reaction (4). **a** Energetic profiles using uB3LYP (green stars) and MP2 (red points) methods with 6–31+G(d,p) basis set. **b** The transition state geometry optimized at uB3LYP/6–31+G(d,p) level of theory with labels of C3-H29. The distance between C3 and H29 is the *x*-axis in (**a**)

In reaction (2), the free radical generated in reaction (1) extracts a hydrogen atom from H_2 and produces a toluene molecule and a hydrogen atom radical. The MEP of reaction (2) using both uB3LYP functional and MP2 methods with 6–31+G(d,p) basis set are plotted in Fig. 5a along the key atomic distances between C12 and H16 forming carbon-hydrogen bond. The geometries of transition states obtained using these two methods have similar key atomic distances (C12-H16) as 1.24 Å and 1.34 Å in uB3LYP and MP2 methods, respectively. The actual reaction process proceeds to the opposite direction to the *x*-axis as the carbon-hydrogen distance decreases. The B3LYP functional underestimates the reaction barrier about 2 kcal/mol comparing to the MP2 results from reactant to transition state progress. However, from transition state to product, the reaction barriers of MP2 method are much lower than the B3LYP method.

In reaction (3), the 2-phenylethyl free radical extracts a hydrogen atom from H_2 to generate ethylbenzene molecule and regenerate a H• radical. The MEP of reaction (3) using B3LYP functional and MP2 methods with 6–31+G(d,p) basis set are plotted in Fig. 6a along the key atomic distance. The key atoms (C15 and H19) forming carbon-hydrogen bond are labeled in Fig. 6b. The geometries of transition state have a similar key atomic distance (C15 and H19) forming carbon-hydrogen bond as 1.37 Å and 1.39 Å in B3LYP and MP2 methods, respectively. The actual reaction process proceeds to the opposite direction to the *x*-axis as the carbon-hydrogen distance decreases. The B3LYP functional underestimates the reaction barrier by 4.05 kcal/mol comparing with the MP2 results. However, the shape of energetic reaction profiles along the key atomic distance are similar between B3LYP and MP2 methods. Despite the difference of energetics, both B3LYP and MP2 methods give similar progress of the reaction.

In reaction (4), DPE binds with a hydrogen atom forming carbon-hydrogen bond to generate a new free radical. The MEP of reaction (4) using B3LYP functional and MP2 methods with 6–31+G(d,p) basis set are plotted in Fig. 7a along the key atomic distance. The key atoms are labeled as C3 and H29 in transition state geometry of reaction (4)
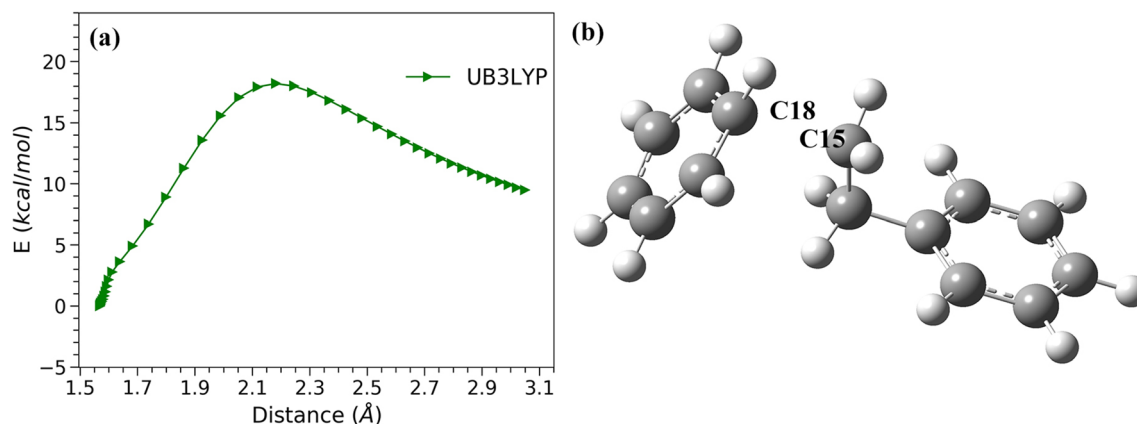

Fig. 8 The minimum energy pathways of reaction (5). **a** Energetic profiles using uB3LYP/6–31+G(d,p) (green stars). **b** The transition state geometry optimized by uB3LYP/6–31+G(d,p) level of theory with labels of C15-H18. The distance between C15 and H18 is the *x*-axis in (**a**)
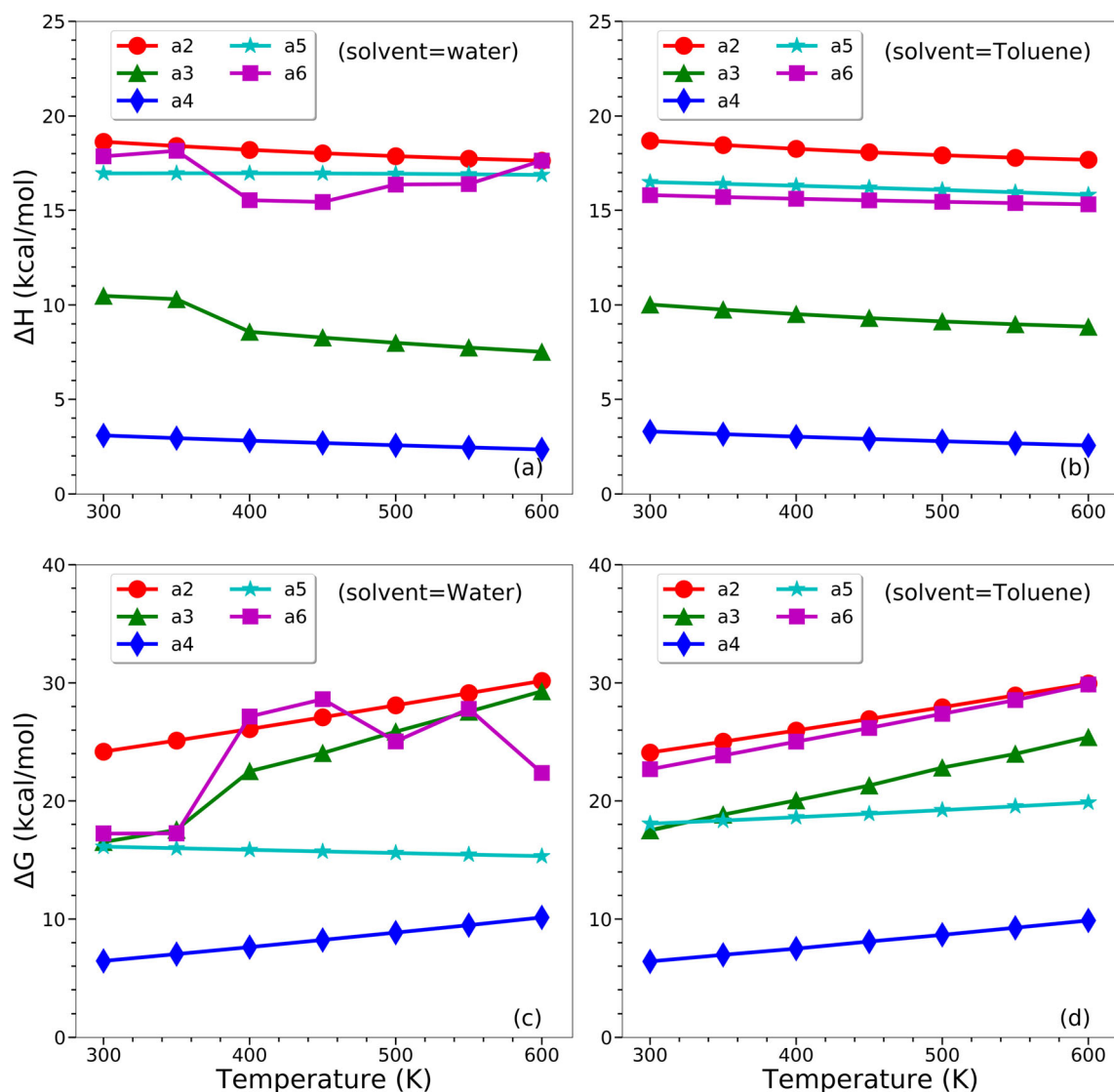
Fig. 9 The free energy barriers and enthalpies of a2, a3, a4, a5, and a6 reactions with different solvents in temperatures range from 0 to 600 K at uB3LYP/6–31+G(d,p) level of theory. **a** Enthalpy barriers with solvent water. **b** Enthalpy barriers with solvent toluene. **c** Free energy barriers with solvent water. **d** Free energy barriers with solvent toluene

illustrated in Fig. 7b. The transition states generated by uB3LYP and MP2 methods are quite different in geometries

Table 3 The temperatures and pressures for water and toluene as solvents

Temperature (K)	Pressures (atm)	
	For water	For toluene
300	1	9.87
350	1	9.87
400	9.87	9.87
450	98.96	9.87
500	986.92	19.74
550	986.92	29.61
600	986.92	39.48

and energy, indicating that this reaction represents a theoretical challenge.

In reaction (5), benzene and toluene are generated by breaking carbon-carbon bond of free radical produced in reaction (3). The MEP of reaction (5) is only calculated at B3LYP/6–31G+(d,p) level of theory, which is plotted in Fig. 8a along the key atomic distance between C15 and C18 as illustrated in Fig. 8b. The barrier of reaction (5) is 18.22 kcal/mol with the key atomic distance as 2.18 Å.

The temperature and solvent dependence of reaction barriers

The temperature dependence of reaction barriers in terms of enthalpy and free energy ((2)–(6)) is investigated in the temperature range from 300 to 600 K with water and toluene as

solvents (Fig. 9). To keep water and toluene in liquid state, the pressures used in the calculations corresponding to the temperatures are listed in the Table 3. Toluene is a common used solvent for extractions in pyrolysis [68], and the reaction barriers in water is calculated as a comparison.

Reaction (2) has the highest enthalpy reaction barrier around 300 K in both water and toluene. The reaction barrier slowly decreases with increasing temperature up to 600 K. The trend for barrier of this reaction in free energy is opposite. The free energy reaction barrier is a minimum around 300 K and increases significantly up to 800 K, showing that the entropic effect is predominant in high temperature. Reaction (3) is similar, but the trend is less prominent. For reaction (3), the barrier in enthalpy remains almost constant along the temperature change. The free energy barrier for reaction (3) in toluene increases moderately after 300 K comparing with reaction (2). However, the free energy for reaction (3) in water decreases moderately from 300 to 600 K.

The enthalpy barriers of reactions (4) moderately decreases from 300 to 600 K and the free energy barriers increase in the temperature range. The trend of decreasing or increasing of reaction (4) are less obvious than the trends in reaction (3). This is probably due to the lack of entropic factor with single hydrogen atom radical.

Reaction (5) shows the most interesting dependency on both temperature and solvent. The enthalpic barrier of this reaction with increasing temperature keep a plateau from 300 up to 600 K. The free energy barrier of reaction (5) slightly decreases in water solvent. However, the trend is completely reversed in toluene. As a key hydrocracking reaction step, reaction (5) seems to be a good candidate as a target to optimize hydrocracking efficiency.

The overall entropy barriers of reaction (6) in water have an increasing trend in temperature range from 300 to 600 K. The barriers at 400 K and 450 K are lower than the barriers at other temperatures. At 600 K, the barrier has the highest value. However, all the entropy barriers of reaction (6) in water are

around 17 kcal/mol, which means that the increments or decrements on the barriers are small. Meanwhile, the free energy reaction barriers of reaction (6) in water solvent increase from temperature 300 to 450 K and has obvious fluctuations when the temperatures are higher than 450 K. The lowest free energy barrier occurs at 600 K. The free energy barriers of reaction (6) in toluene as solvent keeps increasing towards high temperature. The fluctuated free energy barriers of reaction (6) in water are suspected due to the pressures and temperatures used to maintain the liquid phase of water. The entropies of reaction (6) in water are sensitive to the parameters including temperatures, pressures, and volumes of the system. In the temperature range from 300 to 450 K, the entropy barriers heavily depend on the temperatures, therefore the free energy barriers increase with the increasing temperature. From temperature 500 to 600 K, the pressure and volume are more dominant parameters. So, the free energy barriers have the fluctuations under their combined contributions illustrated in Fig. 9c.

In addition, the temperature dependence of reaction barriers in terms of enthalpy and free energy ((2)–(6)) is investigated in the temperature range from 0 to 1000 K in vacuum (Fig. 10). For reactions (2), (3), (4), (6), the enthalpy barriers have a maximum at 50 K and moderately decrease from 100 to 1000 K. The enthalpy barriers of reaction (5) have no obvious trend and seems be constant in the whole temperature (0 to 1000 K). The free energy barriers of reactions (2), (3), (4), (6) have a converse trend with their curves of enthalpies. They have a decrement at 50 K and keep increasing in temperature range from 100 to 1000 K. Reaction (4) has a lower increasing slope than reactions (2), (3), (6). It has a lower increasing slope comparing with reactions (2), (3), (6). The free energy barrier of reaction (5) decreases slightly in the temperature range from 0 to 1000 K.

Although PCM was not parametrized for wide range of temperature usage, there are some computational studies about temperature dependence of chemical systems using
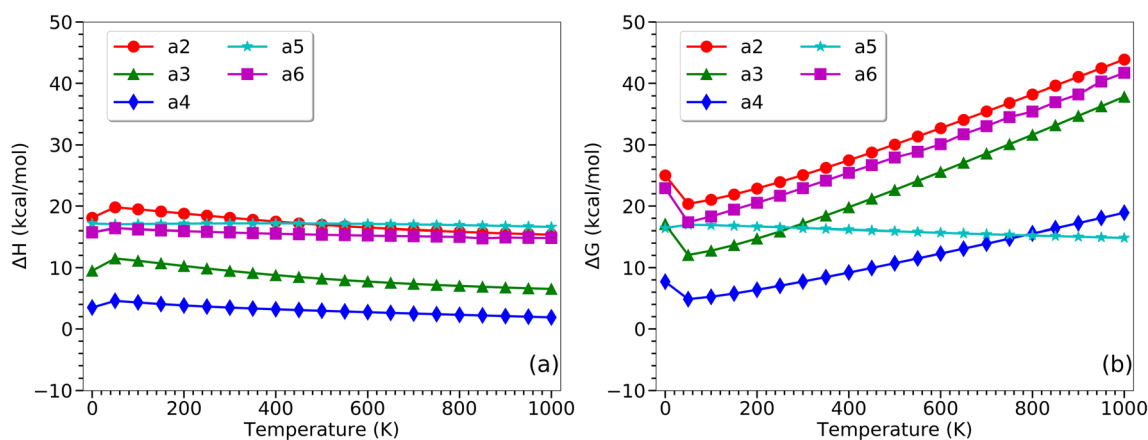

Fig. 10 The enthalpies (a) and free energy (b) barriers of a2, a3, a4, a5, and a6 reactions in vacuum in temperatures range from 0 to 1000 K at uB3LYP/6–31+G(d,p) level of theory

PCM [69–71]. Our temperature calculations do provide some reasonable indication about the general trend of reaction energies regarding temperature changes and should be considered as a valuable guidance about the target reactions.

Summary

The DPE thermal cracking mechanism is represented by initiation, H-transfer, H-ipso, and termination reactions. The key energies including barriers and overall reaction energies of representing reactions were calculated at various levels of theory, including B3LYP, MP2, CBS-QB3, and CCSD. Single point calculations with large basis sets were also carried out. In addition, detailed reaction pathways of these reactions were investigated using IRC method and DFT and MP2 methods. Both temperature and solvent dependency of the reaction barriers of these reactions were investigated in details. Key reactions with either prominent temperature dependency or solvent dependency were identified. The temperature dependence of the enthalpy and free energy barriers in the high temperature range revealed the importance of the entropic contribution and provided valuable information for future optimization in petroleum thermal cracking industry. As summary, the detailed quantum chemistry calculations of the DPE thermal cracking reaction provides great insight into the asphaltene thermal cracking mechanisms and could be used to further improve the petroleum thermal cracking efficiency.

References

1. Long RB, Speight JG (1997) The composition of petroleum. Petroleum chemistry and refining1st edn. CRC Press, Boca Raton, pp 1–38
2. Speight JG (2015) Handbook of petroleum product analysis. Hoboken, New Jersey
3. McCain Jr WD (2017) Properties of petroleum fluids. Tulsa, Oklahoma
4. Speight JG (2003) Thermal cracking of petroleum. Natural and laboratory-simulated thermal geochemical processes. Springer, Dordrecht, pp 31–52
5. Speight JG (2014) The chemistry and technology of petroleum. **Boca Raton**
6. Speight J (2004) Petroleum asphaltenes-part 1: asphaltenes, resins and the structure of petroleum. Oil Gas Sci. Technol. 59(5):467–477. https://dx.doi.org/10.2516/ogst:2004032
7. Hurd CD (1929) The pyrolysis of carbon compounds, New York
8. Fabuss B, Smith J, Lait R, Fabuss M, Satterfield C (1964) Kinetics of thermal cracking of paraffinic and naphthenic fuels at elevated pressures. Industrial & Engineering Chemistry Process Design and Development 3(1):33–37. https://doi.org/10.1021/i260009a009
9. Eliel EL, Wilen SH, Mander LN (1994) Stereochemistry of organic compounds, vol vol 13. Wiley & Sons, Inc., New York, pp 991–1118
10. ElGalad M, El-Khatib K, Abdelkader E, El-Araby R, ElDiwani G, Hawash S (2018) Empirical equations and economical study for blending biofuel with petroleum jet fuel. J. Adv. Res. 9:43–50. https://doi.org/10.1016/j.jare.2017.10.005
11. Brouwer D, Hogeveen H (1972) Electrophilic substitutions at alkanes and in alkylcarbonium ions. Prog. Phys. Org. Chem. 9:179–240. https://doi.org/10.1002/9780470171882.ch4
12. Ungerer P (1990) State of the art of research in kinetic modelling of oil formation and expulsion. Org. Geochem. 16(1–3):1–25. https://doi.org/10.1016/0146-6380(90)90022-R
13. Poutsma M (1976) Mechanistic considerations of hydrocarbon transformations catalyzed by zeolites. American Chemical Society, Washington, DC
14. Park H-B, Kim K-D, Lee Y-K (2018) Promoting asphaltene conversion by tetralin for hydrocracking of petroleum pitch. Fuel 222:105–113. https://doi.org/10.1016/j.fuel.2018.02.154
15. Greensfelder B, Voge H, Good G (1949) Catalytic and thermal cracking of pure hydrocarbons: mechanisms of reaction. Ind. Eng. Chem. 41(11):2573–2584. https://doi.org/10.1021/ie50479a043
16. Maihom T, Pantu P, Tachakritikul C, Probst M, Limtrakul J (2010) Effect of the zeolite nanocavity on the reaction mechanism of n-hexane cracking: a density functional theory study. J. Phys. Chem. C 114(17):7850–7856. https://doi.org/10.1021/jp911732p
17. Wu G, Katsumura Y, Matsuura C, Ishigure K, Kubo J (1996) Comparison of liquid-phase and gas-phase pure thermal cracking of n-hexadecane. Ind. Eng. Chem. Res. 35(12):4747–4754. https://doi.org/10.1021/ie960280k
18. Kaminski T, Husein MM (2018) Thermal cracking of atmospheric residue versus vacuum residue. Fuel Process. Technol. 181:331–339. https://doi.org/10.1016/j.fuproc.2018.10.014
19. Corma A, Sauvanaud L, Mathieu Y, Al-Bogami S, Bourane A, Al-Ghrami M (2018) Direct crude oil cracking for producing chemicals: thermal cracking modeling. Fuel 211:726–736. https://doi.org/10.1016/j.fuel.2017.09.099
20. Alshareef AH, Scherer A, Tan X, Azyat K, Stryker JM, Tykwinski RR, Gray MR (2011) Formation of archipelago structures during thermal cracking implicates a chemical mechanism for the formation of petroleum asphaltenes. Energy Fuel 25(5):2130–2136. https://doi.org/10.1021/ef200170a
21. Bounaceur R, Scacchi G, Marquaire P-M, Dominé F (2000) Mechanistic modeling of the thermal cracking of tetralin. Ind. Eng. Chem. Res. 39(11):4152–4165. https://doi.org/10.1021/ie000276f
22. Rakotoalimanana DA, Bounaceur R, Béhar F, Burklé-Vitzthum V, Marquaire P-M (2016) Thermal cracking of n-butylcyclohexane at high pressure (100 bar)—part 2: mechanistic modeling. J. Anal. Appl. Pyrolysis 120:174–185. https://doi.org/10.1016/j.jaap.2016.05.003
23. Montoya T, Argel BL, Nassar NN, Franco CA, Cortés FB (2016) Kinetics and mechanisms of the catalytic thermal cracking of asphaltenes adsorbed on supported nanoparticles. Pet. Sci. 13(3):561–571
24. Swisher JA, Hansen N, Maesen T, Keil FJ, Smit B, Bell AT (2010) Theoretical simulation of n-alkane cracking on zeolites. J. Phys. Chem. C 114(22):10229–10239
25. Taketsugu T, Gordon MS (1995) Dynamic reaction path analysis based on an intrinsic reaction coordinate. J. Chem. Phys. 103(23):10042–10049. https://doi.org/10.1063/1.470704
26. Mennucci B, Tomasi J, Cammi R, Cheeseman J, Frisch M, Devlin F, Gabriel S, Stephens P (2002) Polarizable continuum model (PCM) calculations of solvent effects on optical rotations of chiral

molecules. J. Phys. Chem. A 106(25):6102–6113. https://doi.org/10.1021/jp020124t

27. van der Vaart A, Karplus M (2007) Minimum free energy pathways and free energy profiles for conformational transitions based on atomistic molecular dynamics simulations. J. Chem. Phys. 126(16):164106. https://doi.org/10.1063/1.2719697

28. Petrone A, Cimino P, Donati G, Hratchian HP, Frisch MJ, Rega N (2016) On the driving force of the excited-state proton shuttle in the green fluorescent protein: a time-dependent density functional theory (TD-DFT) study of the intrinsic reaction path. J. Chem. Theory Comput. 12(10):4925–4933

29. Smith CM, Savage PE (1994) Reactions of polycyclic alkylaromatics—VI. Detailed chemical kinetic modeling. Chem. Eng. Sci. 49(2):259–270. https://doi.org/10.1016/0009-2509(94)80043-X

30. Cardozo SD, Schulze M, Tykwinski RR, Gray MR (2015) Addition reactions of olefins to asphaltene model compounds. Energy Fuel 29(3):1494–1502. https://doi.org/10.1021/ef502616v

31. Santos Silva H, Alfarra A, Vallverdu G, Bégué D, Bouyssiere B, Baraille I (2018) Impact of H-bonds and porphyrins on asphaltene aggregation as revealed by molecular dynamics simulations. Energy Fuel 32(11):11153–11164. https://doi.org/10.1021/acs.energyfuels.8b01901

32. Badran I, Nassar NN, Marei NN, Hassan A (2016) Theoretical and thermogravimetric study on the thermo-oxidative decomposition of Quinolin-65 as an asphaltene model molecule. RSC Adv. 6(59):54418–54430. https://doi.org/10.1039/C6RA07761G

33. Qi X, Wang D, Xin H, Qi G (2013) In situ FTIR study of real-time changes of active groups during oxygen-free reaction of coal. Energy Fuel 27(6):3130–3136. https://doi.org/10.1021/ef400534f

34. Qi X, Chen L, Xin H, Ji Y, Bai C, Song R, Xue H, Liu F (2018) Reaction mechanism and thermodynamic properties of aliphatic hydrocarbon groups during coal self-heating. Energy Fuel 32(10):10469–10477. https://doi.org/10.1021/acs.energyfuels.8b02165

35. Rice F (1933) The thermal decomposition of organic compounds from the standpoint of free radicals III. The calculation of the products formed from paraffin hydrocarbons. J Am Chem Soc 55(7):3035–3040. https://doi.org/10.1021/ja01334a075

36. Kossiakoff A, Rice FO (1943) Thermal decomposition of hydrocarbons, resonance stabilization and isomerization of free radicals1. J. Am. Chem. Soc. 65(4):590–595. https://doi.org/10.1021/ja01244a028

37. Huang X, Gu J, Cheng D-G, Chen F, Zhan X (2013) Pathways of liquefied petroleum gas pyrolysis in hydrogen plasma: a density functional theory study. Journal of Energy Chemistry 22(3):484–492. https://doi.org/10.1016/S2095-4956(13)60063-7

38. Hao H, Lian P, Gong J, Gao R (2018) Theoretical study on the hydrogenation mechanisms of model compounds of heavy oil in a plasma-driven catalytic system. Catalysts 8(9):381. https://doi.org/10.3390/catal8090381

39. Xiao Y, Longo J, Hieshima G, Hill R (1997) Understanding the kinetics and mechanisms of hydrocarbon thermal cracking: an ab initio approach. Ind. Eng. Chem. Res. 36(10):4033–4040. https://doi.org/10.1021/ie960724c

40. Schiesser C, Skidmore M (1999) An ab initio study of β-fragmentation reactions in some alkoxyacyl (alkoxycarbonyl) and related radicals. J. Chem. Soc. Perkin Trans. 2(10):2041–2047. https://doi.org/10.1039/A904809J

41. Hunter KC, East AL (2002) Properties of C−C bonds in n-alkanes: relevance to cracking mechanisms. J. Phys. Chem. A 106(7):1346–1356. https://doi.org/10.1021/jp0129030

42. Raucci U, Savarese M, Adamo C, Ciofini I, Rega N (2015) Intrinsic and dynamical reaction pathways of an excited state proton transfer. J. Phys. Chem. B 119(6):2650–2657. https://doi.org/10.1021/jp508947f

43. Tsutsumi T, Ono Y, Arai Z, Taketsugu T (2018) Visualization of the intrinsic reaction coordinate and global reaction route map by classical multidimensional scaling. J. Chem. Theory Comput. 14(8):4263–4270. https://doi.org/10.1021/acs.jctc.8b00176

44. Gray MR (2003) Consistency of asphaltene chemical structures with pyrolysis and coking behavior. Energy Fuel 17(6):1566–1569. https://doi.org/10.1021/ef030015t

45. Girdler R (1965) Constitution of asphaltenes and related studies. In: Assoc Asphalt Paving Technol Proc:45–79

46. Moschopedis SE, Fryer JF, Speight JG (1976) Investigation of asphaltene molecular weights. Fuel 55(3):227–232. https://doi.org/10.1016/0016-2361(76)90093-4

47. Kawai H, Kumata F (1998) Free radical behavior in thermal cracking reaction using petroleum heavy oil and model compounds. Catal. Today 43(3–4):281–289. https://doi.org/10.1016/S0920-5861(98)00157-6

48. Guthrie RD (2000) Thermolysis of organic compounds under H2 (D2). J. Anal. Appl. Pyrolysis 54(1–2):89–107. https://doi.org/10.1016/S0165-2370(99)00080-7

49. Hohenberg P, Kohn W (1964) Inhomogeneous electron gas. Phys. Rev. 136(3B):B864. https://doi.org/10.1103/PhysRev.136.B864

50. Kohn W, Sham LJ (1965) Self-consistent equations including exchange and correlation effects. Phys. Rev. 140(4A):A1133. https://doi.org/10.1103/PhysRev.140.A1133

51. Parr RG (1980) Density functional theory of atoms and molecules. Horizons of quantum chemistry. Springer, Dordrecht, pp 5–15. https://doi.org/10.1007/978-94-009-9027-2_2

52. Salahub DR (1989) The challenge of d and f electrons: theory and computation. In. ACS Symposium Series. American Chemical Society. https://doi.org/10.1021/bk-1989-0394.fw001

53. Frisch MJ, Head-Gordon M, Pople JA (1990) A direct MP2 gradient method. Chem. Phys. Lett. 166(3):275–280. https://doi.org/10.1016/0009-2614(90)80029-D

54. Frisch MJ, Head-Gordon M, Pople JA (1990) Semi-direct algorithms for the MP2 energy and gradient. Chem. Phys. Lett. 166(3):281–289. https://doi.org/10.1016/0009-2614(90)80030-H

55. Head-Gordon M, Pople JA, Frisch MJ (1988) MP2 energy evaluation by direct methods. Chem. Phys. Lett. 153(6):503–506. https://doi.org/10.1016/0009-2614(88)85250-3

56. Sæbø S, Almlöf J (1989) Avoiding the integral storage bottleneck in LCAO calculations of electron correlation. Chem. Phys. Lett. 154(1):83–89. https://doi.org/10.1016/0009-2614(89)87442-1

57. Head-Gordon M, Head-Gordon T (1994) Analytic MP2 frequencies without fifth-order storage. Theory and application to bifurcated hydrogen bonds in the water hexamer. Chem. Phys. Lett. 220(1–2):122–128. https://doi.org/10.1016/0009-2614(94)00116-2

58. Čížek J (1969) On the use of the cluster expansion and the technique of diagrams in calculations of correlation effects in atoms and molecules. Adv. Chem. Phys.:35–89. https://doi.org/10.1002/9780470143599.ch2

59. Purvis III GD, Bartlett RJ (1982) A full coupled-cluster singles and doubles model: the inclusion of disconnected triples. J. Chem. Phys. 76(4):1910–1918. https://doi.org/10.1063/1.443164

60. Scuseria GE, Janssen CL, Schaefer Iii HF (1988) An efficient reformulation of the closed-shell coupled cluster single and double excitation (CCSD) equations. J. Chem. Phys. 89(12):7382–7387. https://doi.org/10.1063/1.455269

61. Scuseria GE, Schaefer III HF (1989) Is coupled cluster singles and doubles (CCSD) more computationally intensive than quadratic configuration interaction (QCISD)? J. Chem. Phys. 90(7):3700–3703. https://doi.org/10.1063/1.455827

62. Montgomery Jr JA, Frisch MJ, Ochterski JW, Petersson GA (2000) A complete basis set model chemistry VII. Use of the minimum population localization method. J Chem Phys 112(15):6532–6542. https://doi.org/10.1063/1.481224

63. Montgomery Jr JA, Frisch MJ, Ochterski JW, Petersson GA (1999) A complete basis set model chemistry VI. Use of density functional geometries and frequencies. J Chem Phys 110(6):2822–2827. https://doi.org/10.1063/1.477924

64. Fukui K (1981) The path of chemical reactions-the IRC approach. Acc. Chem. Res. 14(12):363–368. https://doi.org/10.1021/ar00072a001

65. Hratchian H, Schlegel H (2005) Theory and applications of computational chemistry: the first 40 years Dykstra, CE:195-249

66. Frisch MJ, Trucks GW, Schlegel HB, Scuseria GE, Robb MA, Cheeseman JR, Scalmani G, Barone V, Petersson GA, Nakatsuji H, Li X, Caricato M, Marenich AV, Bloino J, Janesko BG, Gomperts R, Mennucci B, Hratchian HP, Ortiz JV, Izmaylov AF, Sonnenberg JL, Williams, Ding F, Lipparini F, Egidi F, Goings J, Peng B, Petrone A, Henderson T, Ranasinghe D, Zakrzewski VG, Gao J, Rega N, Zheng G, Liang W, Hada M, Ehara M, Toyota K, Fukuda R, Hasegawa J, Ishida M, Nakajima T, Honda Y, Kitao O, Nakai H, Vreven T, Throssell K, Montgomery Jr. JA, Peralta JE, Ogliaro F, Bearpark MJ, Heyd JJ, Brothers EN, Kudin KN, Staroverov VN, Keith TA, Kobayashi R, Normand J, Raghavachari K, Rendell AP, Burant JC, Iyengar SS, Tomasi J, Cossi M, Millam JM, Klene M, Adamo C, Cammi R, Ochterski JW, Martin RL, Morokuma K, Farkas O, Foresman JB, Fox DJ (2016) Gaussian 16 rev. B.01 Wallingford, CT

67. Vernon LW (1980) Free radical chemistry of coal liquefaction: role of molecular hydrogen. Fuel 59(2):102–106. https://doi.org/10.1016/0016-2361(80)90049-6

68. Marsh H, Martínez-Escandell M, Rodríguez-Reinoso F (1999) Semicokes from pitch pyrolysis: mechanisms and kinetics. Carbon 37 (3):363–390. doi:https://doi.org/10.1016/S0008-6223(98)00205-X

69. Pham HH, Taylor CD, Henson NJ (2013) First-principles prediction of the effects of temperature and solvent selection on the dimerization of benzoic acid. J. Phys. Chem. B 117(3):868–876. https://doi.org/10.1021/jp3062465

70. Gupta M, Svendsen HF, Silva EFD (2010) Temperature sensitivity of piperazine and its derivatives using polarizable continuum solvation model. 2010 2nd International Conference on Chemical, Biological and Environmental Engineering, 2–4 Nov. 2010:386–390. https://doi.org/10.1109/ICBEE.2010.5653461

71. Balevicius V, Balevicius VJ, Aidas K, Fuess H (2007) Determination of critical indices by "slow" spectroscopy: NMR shifts by statistical thermodynamics and density functional theory calculations. J. Phys. Chem. B 111(10):2523–2532. https://doi.org/10.1021/jp065477x